Double Andreev reflections in type-II Weyl semimetal-superconductor junctions

Zhe Hou[1] and Qing-Feng Sun[1,2,*]

[1]*International Center for Quantum Materials, School of Physics, Peking University, Beijing 100871, China*

[2]*Collaborative Innovation Center of Quantum Matter, Beijing 100871, China*

(Received 3 May 2017; revised manuscript received 30 September 2017; published 20 October 2017)

We study the Andreev reflections (ARs) at the interface of the type-II Weyl semimetal-superconductor junctions and find double ARs when the superconductor is put in the Weyl semimetal band tilting direction, which is similar to the double reflections of light in anisotropic crystals. The directions of the double (retro and specular) ARs are symmetric about the normal due to the hyperboloidal Fermi surface near the Weyl nodes, but with different AR amplitudes depending on the incident electron. When the normal direction of the Weyl semimetal-superconductor interface is changed from parallel to perpendicular with the band tilt, the double ARs gradually evolve into one retro-AR and one normal reflection, resulting in an anisotropic differential conductance, which is a unique observable signature for the double ARs in experiments.

DOI: 10.1103/PhysRevB.96.155305

I. INTRODUCTION

In condensed matter physics, massless Dirac fermions or chiral Weyl fermions exist as low-energy excitations and exhibit many novel phenomena in quantum transport [1–9], triggering much interest in exploring new quasiparticles in real quantum systems [10–12]. Materials hosting Weyl fermions are called Weyl semimetals (WSMs), where the conduction and valence bands have crossing points in the bulk, known as the "Weyl nodes." The spectrum around the Weyl node is coniclike, similar to the two-dimensional Dirac cones in graphene [1]. Since all three Pauli matrices are used in the Weyl Hamiltonian, the Weyl points are very robust against weak time-reversal symmetry breaking or inversion-symmetry breaking perturbations. The only symmetry allowed to preserve the Weyl node is the translation symmetry of the crystal lattice. In the momentum space, the Weyl node acts like a topological charge with the charge sign corresponding to its chirality. Due to this topological property, the Fermi arcs that connect the Weyl nodes with different chiralities can be observed on the surface of a Weyl semimetal.

WSMs with a pointlike Fermi surface are referred as the conventional or type-I WSMs. But recent progresses show that the conic spectrum can be tilted or overtilted by adding a kinetic term into the energy spectrum to transform the WSM into the type-II one [13,14], where the Fermi surface near the Weyl nodes is hyperboloidal with a large density of states. The dramatic spectrum tilt violates the Lorentz invariance and generates electron and hole pockets near the Weyl nodes. Although the Lorentz symmetry is fundamental in high-energy physics, it is not necessarily present in quantum materials. Due to the coexistence of electron and hole states, some interesting phenomena that are distinct from the type-I WSM have been predicted, e.g., the unusual magnetic quantum oscillations, field-selective anomalous optical conductivity, and anomalous Hall effect [15–20]. Experimentally, LaAlGe, WTe_2, and $MoTe_2$ have been confirmed as the type-II WSMs by observing the topological Fermi arcs between electron and hole pockets using angle-resolved photoemission spectroscopy (ARPES) [21–28] or STM measurement [29]. WSMs can be induced into Weyl superconductor by intrinsic electron-phonon coupling, extrinsic proximity effect with an s-wave superconductor [14,30,31], or by the metallic point contacts [32].

In the conductor-superconductor interface, except for the normal electron reflection, there also exists Andreev reflection (AR) [33], a process where the electron is reflected back as a hole in the conductor and a Cooper-pair is injected into the superconductor. At the small bias, the conductance of the conductor-superconductor junction is mainly determined by the AR [34–36]. ARs can be classified into retro-AR and specular AR according to the directions of the reflected holes. Retro-AR occurs in the normal metal-superconductor interface where the hole almost retraces the path of the incident electron [see Fig. 1(a)] and the electron-hole conversion is intraband, i.e., both electron and hole are located in the same conduction or valence band. In the graphene-superconductor junctions, the electron and reflected hole can locate in different bands, of which the interband conversion results in the specular AR [see Fig. 1(b)] [37–39]. In both cases only single AR (retro or specular AR) occurs at the interface, and the normal reflection exists usually.

One question arises that weather there exists a new kind of AR in type-II WSM-superconductor junctions inspired by the violent band tilt in type-II WSM. Surprisingly, in this paper, we find the double ARs at the type-II WSM-superconductor interface [see Fig. 1(c)], where retro-AR and specular AR happen simultaneously for one incident electron. The physical reason behind the double ARs is that the spectrum tilt makes the conduction and valence bands lie in the same Fermi level, so both intraband and interband electron-hole conversions happen if the superconductor is put in the band tilt direction of the WSM ($+x$ direction). The band tilt also forbids the normal reflection, resulting in a conductance plateau when the bias is within the superconductor gap. Moreover, when the interface orientation of the WSM-superconductor junction is changed from $+x$ direction to $+y$ direction, the double ARs gradually evolve into one retro-AR and one normal reflection with the subgap conductance decreasing with the interface orientation angle, indicating that the ARs or conductance through type-II WSM-superconductor junctions are strongly anisotropic. We propose the anisotropic conductance as a practicable

*sunqf@pku.edu.cn

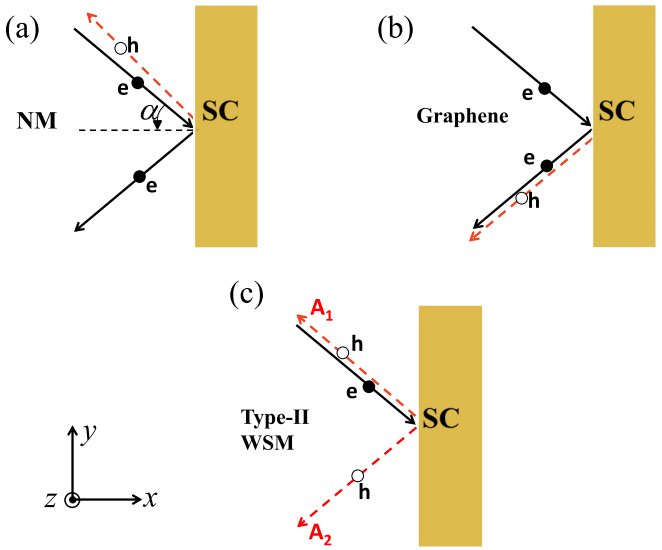

FIG. 1. Schematic diagrams for (a) retro-AR in normal metal-superconductor (NM-SC) interface, (b) specular AR in graphene-superconductor interface, and (c) double ARs in type-II WSM-superconductor interface. The solid black arrows indicate the directions of the incident and reflected electrons, and the dashed red arrows indicate the directions for the reflected holes. In type-II WSM-superconductor interface, normal reflection is prohibited and the holes are reflected in the retro and specular directions of the incident electron.

way to detect the tilting direction of the Weyl cones in experiments.

The rest of the paper is constructed as follows. In Sec. II, we give the theoretical model describing the type-II WSM-superconductor junctions. In Secs. III and IV, we study the double ARs when the WSM-superconductor interface orientation angle $\theta = 0$ and $\theta \neq 0$, respectively. The conductance of the WSM-superconductor junctions is investigated in Sec. V. Section VI gives a brief summary of our results. The detailed derivations of the coefficients of the double ARs in the presence of the interface barrier and the orientation angle $\theta \neq 0$ are put in Appendixes A and B.

II. MODEL AND HAMILTONIAN OF THE TYPE-II WSM-SUPERCONDUCTOR JUNCTION

We first consider a two-band effective Weyl Hamiltonian near the Weyl node K_0 which respects the time-reversal symmetry but breaks inversion symmetry:

$$H_+(\mathbf{k}) = \hbar v_1 k_x \sigma_0 + \hbar v_2 \mathbf{k}\cdot\boldsymbol{\sigma}, \tag{1}$$

where the wave vector $\mathbf{k}$ is the displacement from the Weyl node K_0, σ_0 is the identity matrix, $\boldsymbol{\sigma} = (\sigma_x,\sigma_y,\sigma_z)$ is the Pauli matrix vector, and v_2 is the Fermi velocity with its sign determining the chirality of the node. The spectrum tilt is described by the parameter v_1. Here we set v_1, v_2 to be positive, and $v_1 > v_2$ to make the WSM being the type-II one. Time reversal symmetry requires another Weyl node locating at $-K_0$ with its effective Hamiltonian satisfying [40]

$$H_-(\mathbf{k}) = -\hbar v_1 k_x \sigma_0 - \hbar v_2 (k_x\sigma_x - k_y\sigma_y + k_z\sigma_z). \tag{2}$$

By substituting $\mathbf{k}$ with $\mathbf{p}/\hbar = -i\nabla_{\mathbf{r}}$, we get the effective Hamiltonian for Weyl nodes at K_0 and $-K_0$ in real space: $H_+(\mathbf{p}/\hbar)$ and $H_-(\mathbf{p}/\hbar)$.

We consider the BCS pairing in the superconductor. Electron excitations near K_0 are coupled by hole excitations near $-K_0$, so the Bogoliubov-de Gennes (BdG) Hamiltonian of the type-II WSM-superconductor junction reads [41]

$$H_{\mathrm{BdG}} = \begin{pmatrix} H_+(\mathbf{p}/\hbar) - \mu(\mathbf{r}) & \Delta(\mathbf{r}) \\ \Delta^*(\mathbf{r}) & -H_-^*(\mathbf{p}/\hbar) + \mu(\mathbf{r}) \end{pmatrix}, \tag{3}$$

where $\mu(\mathbf{r})$, $\Delta(\mathbf{r})$ are the chemical potential and the pairing potential, respectively. One can verify that $H_-^*(\mathbf{p}/\hbar) = H_+(\mathbf{p}/\hbar)$ because of the time-reversal symmetry. $\mu(\mathbf{r})$ and $\Delta(\mathbf{r})$ are step functions:

$$\mu(\mathbf{r}) = \begin{cases} \mu & x < -y\tan\theta \\ U & x > -y\tan\theta \end{cases}, \quad \Delta(\mathbf{r}) = \begin{cases} 0 & x < -y\tan\theta \\ \Delta & x > -y\tan\theta \end{cases}.$$

In the WSM region ($x < -y\tan\theta$), the potential μ is tuned by a gate voltage and the superconductor gap is zero. On the other side, it is the superconducting region ($x > -y\tan\theta$) with a nonzero superconductor gap Δ and a large electrostatic potential U ($U \gg \mu, \Delta$). Here, θ is the intersection angle of the normal of the WSM-superconductor junction interface with the x bias [see Fig. 8(a)].

III. THE DOUBLE ANDREEV REFLECTIONS WHEN THE ORIENTATION ANGLE $\theta = 0$

In this section, we consider the case of the interface orientation angle $\theta = 0$. Then, the WSM and superconductor are in $x < 0$ and $x > 0$ regions, respectively. By solving the eigenvalues of H_{BdG}, we obtain the energy dispersions for electron and hole excitations in the type-II WSM:

$$E_{e\pm}(\mathbf{k}) = \hbar v_1 k_x \pm \hbar v_2 |\mathbf{k}| - \mu, \tag{4}$$

$$E_{h\pm}(\mathbf{k}) = -\hbar v_1 k_x \pm \hbar v_2 |\mathbf{k}| + \mu, \tag{5}$$

and the excitation energy in the superconductor

$$E_s(\mathbf{k}) = \sqrt{\Delta^2 + (\hbar v_1 k_x \pm \hbar v_2 |\mathbf{k}| - U)^2}, \tag{6}$$

with $|\mathbf{k}| = \sqrt{k_x^2 + k_y^2 + k_z^2}$. Denote E_{e+} (E_{h-}) as the conduction band for electron (hole), and E_{e-} (E_{h+}) for the valence band. The band tilt makes the slopes in the $+x$ direction of the bands for electrons (holes) all positive (negative), so there are two incident modes for electrons and two reflected modes for holes. Here we first consider the electron incident from the valence band (E_{e-}). The holes are then reflected into the conduction band (E_{h-}) and the valence band (E_{h+}). The intraband electron-hole conversion results in the retro-AR (A_1) and the interband conversion is for the specular AR (A_2) [see Fig. 1(c)]. So at the type-II WSM-superconductor interface, a beam of incident electron is Andreev reflected into two beams of holes, which is similar to the double reflections of light in anisotropic crystals [42,43].

In the momentum space, the equienergy surfaces (Fermi surfaces) of the type-II WSM for electrons and holes are circular hyperboloids satisfying the equation $\frac{(k_x - k_{xc\pm})^2}{a_\pm^2} - \frac{k_y^2 + k_z^2}{b_\pm^2} = 1$, where $k_{xc\pm} = \frac{(\mu\pm E)v_1}{\hbar(v_1^2 - v_2^2)}$, $a_\pm = \frac{|\mu\pm E|v_2}{\hbar(v_1^2 - v_2^2)}$, $b_\pm = \frac{|\mu\pm E|}{\hbar\sqrt{(v_1^2 - v_2^2)}}$, and

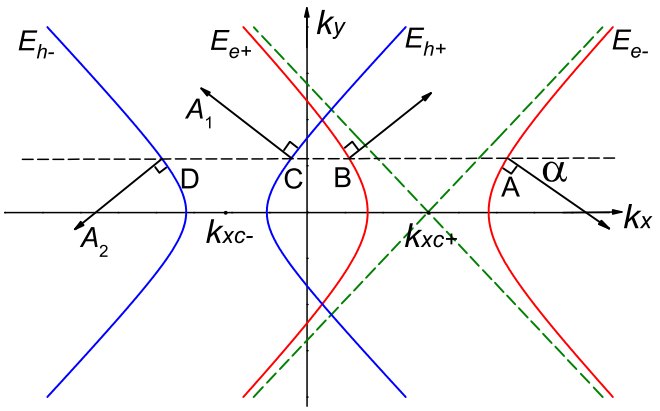

FIG. 2. Hyperbolic equienergy lines ($E_{e\pm}, E_{h\pm}$) for electrons and holes in the k_x-k_y plane in the WSM side. Here $k_z = 0$. The green dashed lines are the asymptotes for $E_{e\pm}$. The intersections of the horizontal dashed line with equienergy lines A, B, C, D denote the incident modes for electrons and reflected modes for holes. The black arrows at A and B denote the directions of the incident electron, and the arrows at C and D are the directions for the double ARs. Here we choose point A as the incident electron mode with an incident angle α, the holes are then reflected in the retro-direction A_1 and the specular direction A_2.

"+" for electrons, "−" for holes. During the reflection process, the energy E and the wave vectors k_y and k_z remain invariant. Since the equienergy surface has rotational symmetry along the k_x axis, for simplicity, we set $k_z = 0$ in the following analysis. Then in the $k_x - k_y$ plane, the equienergy lines become hyperbolas as shown in Fig. 2. Given the energy E and the wave vector k_y, the intersections A, B, C, D denote the modes for the incident electron and the reflected holes in the WSM side with their semiclassical velocity $(v_x, v_y) \equiv \nabla_{\mathbf{k}} E(\mathbf{k})/\hbar$ [$E(\mathbf{k})$ is the energy dispersion for electrons or holes] being perpendicular with the equienergy lines. The black arrow at point A denotes the direction for the incident electron with an incident angle α ($\alpha = -\arctan v_y/v_x$), and the arrows at C and D are the directions for retro-AR (A_1) and specular AR (A_2). E_{h+} and E_{h-} is symmetric about $k_x = k_{xc-}$, so A_1 and A_2 have opposite reflection angles. With increasing wave vector $|k_y|$, the incident angle $|\alpha|$ increases but saturates at a critical angle $\alpha_c = \arctan(v_2/\sqrt{v_1^2 - v_2^2})$.

A. The wave functions in the type-II WSM and superconductor regions

In order to calculate the double AR coefficients A_1 and A_2, we first solve the wave functions in the WSM and superconductor regions, respectively. The BdG equation in the type-II WSM side ($x < 0$) is

$$\begin{pmatrix} H_+(\mathbf{p}/\hbar) - \mu & 0 \\ 0 & -H_+(\mathbf{p}/\hbar) + \mu \end{pmatrix} \begin{pmatrix} f \\ g \end{pmatrix} = E \begin{pmatrix} f \\ g \end{pmatrix}, \quad (7)$$

where f and g are the electron and hole wave functions. At a given incident energy E and the wave vectors k_y, k_z in the y,z direction, the eigenstates are

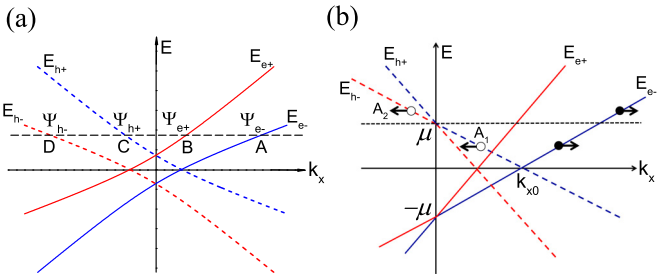

FIG. 3. (a) Dispersion relations for electrons and holes in the type-II WSM with finite k_y or k_z. E_{e+} (E_{h-}) denotes the tilted conduction band for electrons (holes), and E_{e-} (E_{h+}) is the tilted valence band for electrons (holes). The intersections of the black dashed line with the bands denote the incident modes $\Psi_{e\pm}$ for electrons and the reflected modes $\Psi_{h\pm}$ for holes. (b) Dispersion relation at normal incidence ($k_y = k_z = 0$) with the incident angle $\alpha = 0$. The intersection of E_{e-} with the k_x-axis is $k_{x0} = \frac{\mu}{\hbar(v_1 - v_2)}$. The holes are reflected into the modes that are symmetric with the incident modes of electrons about $k_x = k_{x0}$.

$$\begin{aligned}
\Psi_{e+}(\mathbf{r}) &= \begin{pmatrix} k_+ + k_z \\ k_{x+} + ik_y \\ 0 \\ 0 \end{pmatrix} \exp(ik_{x+}x + ik_y y + ik_z z), \\
\Psi_{e-}(\mathbf{r}) &= \begin{pmatrix} -k_- + k_z \\ k_{x-} + ik_y \\ 0 \\ 0 \end{pmatrix} \exp(ik_{x-}x + ik_y y + ik_z z), \\
\Psi_{h+}(\mathbf{r}) &= \begin{pmatrix} 0 \\ 0 \\ -k'_+ + k_z \\ k'_{x+} + ik_y \end{pmatrix} \exp(ik'_{x+}x + ik_y y + ik_z z), \\
\Psi_{h-}(\mathbf{r}) &= \begin{pmatrix} 0 \\ 0 \\ k'_- + k_z \\ k'_{x-} + ik_y \end{pmatrix} \exp(ik'_{x-}x + ik_y y + ik_z z),
\end{aligned} \quad (8)$$

where $\mathbf{r} = (x, y, z)$ and

$$k_{x\pm} = \frac{v_1(E+\mu) \mp v_2\sqrt{(E+\mu)^2 + \hbar^2(v_1^2 - v_2^2)(k_y^2 + k_z^2)}}{\hbar(v_1^2 - v_2^2)},$$

$$k'_{x\pm} = \frac{v_1(\mu - E) \pm v_2\sqrt{(E-\mu)^2 + \hbar^2(v_1^2 - v_2^2)(k_y^2 + k_z^2)}}{\hbar(v_1^2 - v_2^2)},$$

$$k_\pm = \sqrt{k_{x\pm}^2 + k_y^2 + k_z^2},$$

$$k'_\pm = \sqrt{k'^2_{x\pm} + k_y^2 + k_z^2}.$$

The wave functions Ψ_{e+} and Ψ_{e-} are the eigenstates for electrons in the tilted conduction band E_{e+} and valence band E_{e-}. Ψ_{h+} and Ψ_{h-} are the eigenstates for holes in the tilted valence band E_{h+} and conduction band E_{h-}. Figure 3(a) shows the energy dispersions for electrons and holes with finite k_y or k_z. The intersections A, B, C, and D denote the incident and reflected wave functions $\Psi_{e\mp}$, $\Psi_{h\pm}$, and also correspond

to the intersections in Fig. 2. In fact, here k_{x-}, k_{x+}, k'_{x+}, and k'_{x-} are the k_x coordinates of the point A, B, C, and D in Fig. 3(a), respectively. From the slopes of the band dispersions in Fig. 3(a), we can see that both Ψ_{e+} and Ψ_{e-} move in the $+x$ direction, so there are two incident modes for electrons with given energy E and wave vector k_y,k_z. The Andreev reflection is denoted as A_1 (A_2) if the holes are reflected in the mode Ψ_{h+} (Ψ_{h-}).

The superconductor is put in the $x > 0$ region with its BdG equation:

$$\begin{pmatrix} H_+(\mathbf{p}/\hbar) - U & \Delta\sigma_0 \\ \Delta\sigma_0 & -H_+(\mathbf{p}/\hbar) + U \end{pmatrix} \begin{pmatrix} f \\ g \end{pmatrix} = E \begin{pmatrix} f \\ g \end{pmatrix}. \quad (9)$$

In the large U limit, the outgoing wave functions in the superconductor are

$$\Psi_{S+}(\mathbf{r}) = \begin{pmatrix} e^{i\beta} \\ e^{i\beta} \\ 1 \\ 1 \end{pmatrix} \exp(ik_{x1}x + ik_y y + ik_z z - \tau_1 x),$$
$$\Psi_{S-}(\mathbf{r}) = \begin{pmatrix} e^{i\beta} \\ -e^{i\beta} \\ 1 \\ -1 \end{pmatrix} \exp(ik_{x2}x + ik_y y + ik_z z - \tau_2 x), \quad (10)$$

where

$$\beta = \begin{cases} \arccos(E/\Delta) & \text{if} \quad E < \Delta, \\ -i\,\mathrm{arcosh}(E/\Delta) & \text{if} \quad E > \Delta, \end{cases}$$
$$k_{x1} \simeq \frac{U}{\hbar(v_1 + v_2)}, \quad k_{x2} \simeq \frac{U}{\hbar(v_1 - v_2)}, \quad (11)$$
$$\tau_1 = \frac{\Delta \sin\beta}{\hbar(v_1 + v_2)}, \quad \tau_2 = \frac{\Delta \sin\beta}{\hbar(v_1 - v_2)}.$$

The eigenstates $\Psi_{S\pm}(\mathbf{r})$ are the superpositions of electron and hole excitations in the superconductor, which have similar forms as the solutions in the graphene-superconductor junction [37]. When $E > \Delta$, these states propagate in the $+x$ direction, carrying net electron or hole current [44]. When $|E| < \Delta$, $\Psi_{S\pm}(\mathbf{r})$ both decay exponentially as $x \to +\infty$, and the net particle current is zero, so the normal tunneling from the WSM to superconductor is prohibited. In this case, the electron incident from the WSM side can only be normally reflected as an electron or Andreev reflected as a hole. Since no modes exist for the normal electron reflection in the type-II WSM, the Andreev reflection happens with unit probability.

B. The double ARs while without the interface barrier

We first consider Ψ_{e-} as the incident mode. The wave functions $\Psi(\mathbf{r})$ in the WSM region (the $x < 0$ region) can be written as follows:

$$\Psi(\mathbf{r}) = \Psi_{e-}(\mathbf{r}) + r_1\Psi_{h+}(\mathbf{r}) + r_2\Psi_{h-}(\mathbf{r}), \quad (12)$$

where r_1 and r_2 are the reflection amplitudes of the double ARs. The wave functions in the superconductor region (the $x > 0$ region) can be described as

$$\Psi(\mathbf{r}) = a\Psi_{S+}(\mathbf{r}) + b\Psi_{S-}(\mathbf{r}), \quad (13)$$

where a and b are the amplitudes of electronlike and holelike quasiparticles in the superconductor region. Here, r_1, r_2, a, and b are determined by matching the boundary conditions. The matching condition of the wave-functions at $x = 0$ interface of the WSM-superconductor junction is $\Psi(\mathbf{r})|_{x=0^-} = \Psi(\mathbf{r})|_{x=0^+}$. This means

$$[\Psi_{e-}(\mathbf{r}) + r_1\Psi_{h+}(\mathbf{r}) + r_2\Psi_{h-}(\mathbf{r})]_{x=0^-} = [a\Psi_{S+}(\mathbf{r}) + b\Psi_{S-}(\mathbf{r})]_{x=0^+}. \quad (14)$$

Substituting Eqs. (8) and (10) into Eq. (14), we obtain

$$r_{1/2} = \frac{(k_{x-} + ik_y)(k'_{\mp} \pm k_z) \pm (k_- - k_z)(k'_{x\mp} + ik_y)}{(k'_+ - k_z)(k'_{x-} + ik_y) + (k'_{x+} + ik_y)(k'_- + k_z)} e^{-i\beta}.$$

The particle current density operator is defined as

$$J \equiv \frac{1}{\hbar}[r, H_{\mathrm{BdG}}] = \tau_z \otimes [(v_1\sigma_0 + v_2\sigma_x)\mathbf{e}_x + v_2\sigma_y\mathbf{e}_y + v_2\sigma_z\mathbf{e}_z], \quad (15)$$

where $\tau_z = \left(\begin{smallmatrix} 1 & 0 \\ 0 & -1 \end{smallmatrix}\right)$ denotes electron-hole index, and $\mathbf{e}_x$, $\mathbf{e}_y$ and $\mathbf{e}_z$ are unit vectors in x, y, and z directions. Only the x component of the current density operator $J_x = \tau_z \otimes (v_1\sigma_0 + v_2\sigma_x)$ decides the reflection coefficients at the interface. So the Andreev reflection coefficients A_1 and A_2 can be obtained straightforwardly:

$$A_{1/2}(E) \equiv \left|\frac{\langle\Psi_{h\pm}|J_x|\Psi_{h\pm}\rangle}{\langle\Psi_{e-}|J_x|\Psi_{e-}\rangle}\right| |r_{1/2}|^2 = \left|\frac{(k'_{\pm} \mp k_z)(v_1k'_{\pm} \mp v_2k'_{x\pm})}{(k_- - k_z)(v_1k_- - v_2k_{x-})}\right| |r_{1/2}|^2. \quad (16)$$

In addition, one can easily verify that when $k_y = k_z = 0$ (normal incidence), A_1 and A_2 reduce into

$$A_1(E) = \Theta(\mu - E)T^A(E), \quad A_2(E) = \Theta(E - \mu)T^A(E), \quad (17)$$

where Θ is the Heaviside step function and $T^A(E) = 1$ if $E < \Delta$, $T^A(E) = (E - \sqrt{E^2 - \Delta^2})^2/\Delta^2$ if $E > \Delta$. Thus only one AR happens at the normal incidence and A_1, A_2 exchange at the chemical potential μ. From the band structure point of view, the modes symmetry for electrons and holes plays an important role for results Eq. (17). Figure 3(b) is the dispersion relation for the normal incidence ($k_y = k_z = 0$). One can see that the reflected holes only locate in the modes symmetric with the incident modes of the electrons about $k_x = k_{x0}$. When $E < \mu$, the reflected hole is located in the valence band of which the intraband electron-hole conversion results in the retro-AR (A_1). When $E > \mu$, the symmetric reflection modes lie in the conduction band, so A_1 disappears and A_2 arises due to the interband electron-hole conversion. In addition, due to the normal incidence with the incident angle $\alpha = 0$, both the angle α_{A1} of the intraband AR and the angle α_{A2} of the interband AR are zero also. While for a general incidence case with $\alpha \neq 0$, both A_1 and A_2 are nonzero. Importantly, by summing over A_1 and A_2, we find that the total AR coefficient $A \equiv A_1 + A_2 = T^A(E)$, which has the universal form and only depends on the energy E and the superconductor gap Δ, with nothing to do with the incident angle α and other parameters.

In the following numerical calculations, we set $\hbar = 1$, $v_2 = 1$, $\Delta = 1$, and $k_z = 0$. Figure 4(a) shows AR coefficients A_1, A_2, and A versus the incident energy E at the normal incidence

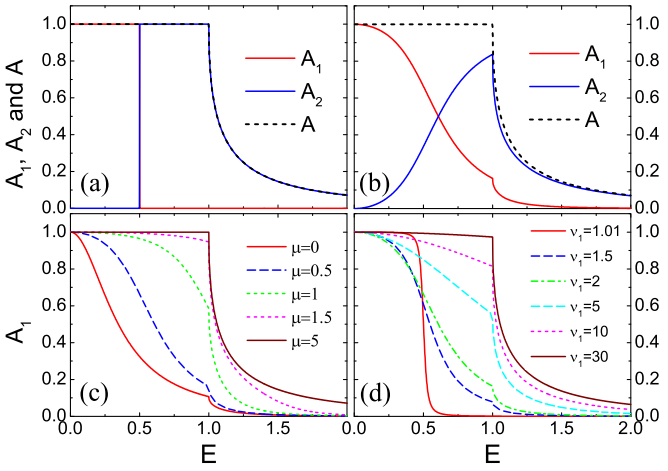

FIG. 4. AR coefficients A_1, A_2, and A as functions of the incident energy E. The parameters are (a) $\mu = 0.5$, $v_1 = 2$, $k_y = 0$; (b) $\mu = 0.5$, $v_1 = 2$, $k_y = 0.2$; (c) $v_1 = 2$, $k_y = 0.2$; and (d) $k_y = 0.2$, $\mu = 0.5$.

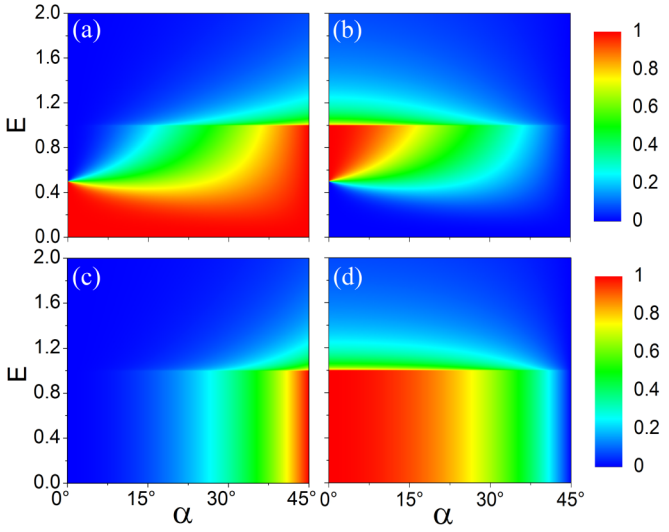

FIG. 5. The incident energy E and incident angle α dependence of the retro-AR A_1 [(a) and (c)] and specular AR A_2 [(b) and (d)] with $v_1 = \sqrt{2}$ and $\mu = 0.5$ [(a) and (b)] and 0 [(c) and (d)].

($\alpha = 0$). The results coincide with Eq. (17) and are attributed to the modes symmetry discussed in Fig. 3(b). For the oblique incidence case ($\alpha \neq 0$), both retro-AR and specular AR happen [see Fig. 4(b)]. When $E = 0$, i.e., at the zero-energy incidence, we find $A_1 = 1$ and $A_2 = 0$. As the energy E increases, the specular AR A_2 goes up and the retro-AR A_1 falls down, and they both get a sharp decline when $E > \Delta$. The total AR coefficient A shows the same variation behaviors in Figs. 4(a) and 4(b) because A only depends on the incident energy E and superconductor gap Δ. In Figs. 4(c) and 4(d), we change the potential μ and the tilt parameter v_1 to see how the retro-AR coefficient A_1 varies. As the potential μ increases, A_1 gets higher and approaches $A_1 = T^A(E)$ in the large μ limit. The retro-AR A_1 also shows the similar asymptotic behavior in the large tilting limit [see $v_1 = 30$ in Fig. 4(d)]. However, when the tilt is very small (see $v_1 = 1.01$), we find $A_1 \simeq \Theta(\mu - E)$, which is similar to the normal incident case.

The incident energy E and incident angle α dependence of the AR coefficients A_1 and A_2 is investigated exhaustively in Fig. 5. The tilt v_1 is chosen to be $\sqrt{2}$, then the incident angle α has an up limit $\alpha_c = 45^\circ$ from the analysis of Fig. 2. Below the chemical potential ($E < \mu$), the retro-AR A_1 first gets down and then goes up to T^A with the increasing of α [see Fig. 5(a)]. While A_1 just increases monotonically with α when $E > \mu$. For the ultimate angle incidence ($\alpha = \alpha_c$), $A_1 = T^A$, and $A_2 = 0$, so only the retro-AR happens. The specular AR A_2 shows the opposite behavior as the retro-AR A_1 due to the relation $A_1 + A_2 = T^A$. Note that for an appropriate incident energy E and angle α, the retro-AR and specular AR, which have opposite reflection angles, happen with nearly equal probabilities (see the green regions in Fig. 5). Another interesting thing we find is that for $\mu = 0$, the retro-AR A_1 and specular AR A_2 are independent of E when $E < \Delta$ [see Figs. 5(c) and 5(d)], which means once the incident angle α is given, the AR coefficients are determined.

Up to now, we have only considered the incident electron from the valence band E_{e-}. Similarly, the AR coefficients A_{1e+} and A_{2e+} for the incident electron from the conduction band E_{e+} can be calculated also [here, A_{1e+} and A_{2e+} are the coefficients for holes reflected into the valence band E_{h+} and the conduction band E_{h-}, respectively]:

$$A_{1/2e+} = \left|\frac{(k'_{\pm} \mp k_z)(v_1 k'_{\pm} \mp v_2 k'_{x\pm})}{(k_+ + k_z)(v_1 k_+ + v_2 k_{x+})}\right| |r_{1/2e+}|^2, \qquad (18)$$

where

$$r_{1/2e+} = \frac{(k_{x+} + ik_y)(k'_{\mp} \pm k_z) \mp (k_+ + k_z)(k'_{x\mp} + ik_y)}{(k'_+ - k_z)(k'_{x-} + ik_y) + (k'_{x+} + ik_y)(k'_- + k_z)} e^{-i\beta}.$$

The results for the conduction band E_{e+} incidence are shown in Fig. 6. One can see that A_{1e+} and A_{2e+} have the same values as A_2 and A_1 in the valence band E_{e-} incidence by comparison with Figs. 4(a) and 4(b), due to the unitarity of the scattering matrix. For the conduction band E_{e+} incidence, the incident direction is symmetric with that of E_{e-} about the normal (see Fig. 2), so A_{1e+} becomes specular AR and A_{2e+} becomes the retro-AR. Therefore, for given energy E and wave vectors k_y and k_z, no matter which incident mode the electron locates in, the coefficient of the specular AR (the retro-AR) has the same values.

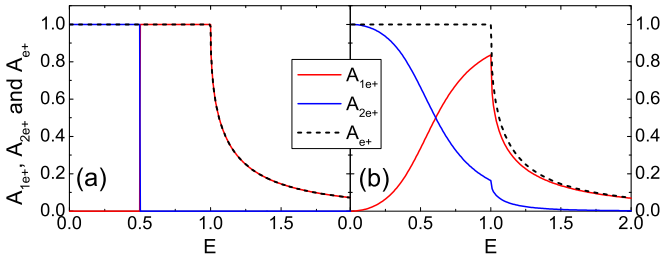

FIG. 6. AR coefficients A_{1e+}, A_{2e+}, and $A_{e+} = A_{1e+} + A_{2e+}$ as functions of the incident energy E for the conduction band E_{e+} incidence. The parameters are $\mu = 0.5$, $v_1 = 2$, $k_y = 0$ in (a) and $\mu = 0.5$, $v_1 = 2$, $k_y = 0.2$ in (b). One can see that A_{1e+} and A_{2e+} have the same values as A_2 and A_1 in the E_{e-} incidence [see Figs. 4(a) and 4(b)].

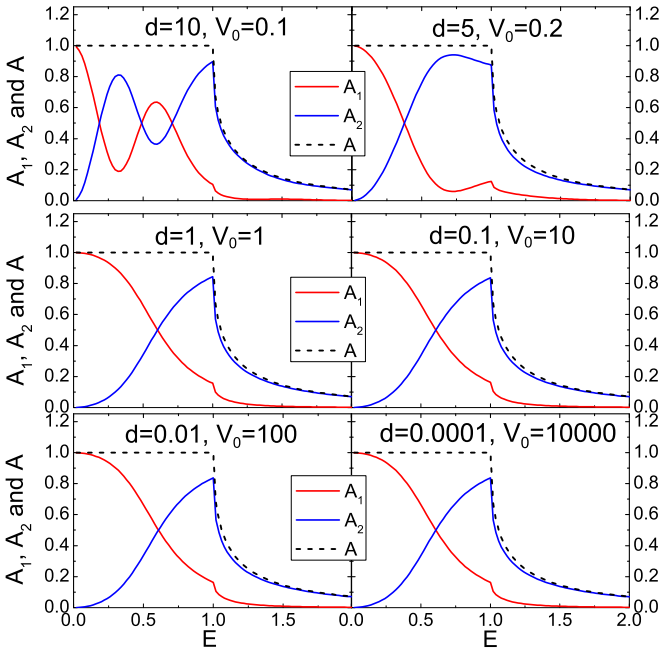

FIG. 7. Double AR coefficients A_1 and A_2 vs the incident energy E for different barrier width d. The barrier strength χ is fixed to 1. The other parameters are the same as Fig. 4(b).

C. Influence of the interface barrier on the double ARs

In this section, we introduce an interface barrier in the type-II WSM-superconductor junction and study the influence of the barrier on the double ARs in detail. A rectangular barrier [45] is considered in the interface and the Hamiltonian is the same with Eq. (3), but the potential $\mu(\mathbf{r})$ has the form

$$\mu(\mathbf{r}) = \begin{cases} \mu, & x < -d \\ -V_0, & -d < x < 0 \\ U, & x > 0 \end{cases}.$$

So the WSM, the barrier, and the superconductor are in $x < -d$, $-d < x < 0$ and $0 < x$ regions, respectively. Here we choose the E_{e-} band as the incident mode for electrons as we have done in Sec. III B.

By calculating the wave functions inside the barrier region and using the matching conditions at interfaces $x = -d$ and $x = 0$ (see Appendix A), we give the numerical results of the AR coefficients A_1, A_2 as functions of the incident energy E in the presence of the rectangular barrier with finite width d and height V_0 (see Fig. 7). Here we fix the barrier strength $\chi = dV_0$ and gradually decrease the barrier width. The other parameters are the same as Fig. 4(b). One can see from Fig. 7 that when $d = 10$, A_1 and A_2 oscillate as varying the incident energy E due to the Fabry-Pérot interference inside the barrier region. With decreasing d, the oscillation gradually disappears (see $d = 5$ in Fig. 7). When the width $d = 1$ (in the order of the wavelength of the incident electron), the values of A_1 and A_2 approach the values in Fig. 4(b). With further decrease of the width d, the AR coefficients A_1 and A_2 do not change almost. In the thin barrier limit ($d \to 0$), the AR coefficients are the same as Fig. 4(b) (see $d < 1$ in Fig. 7), which is also consistent with the analytical derivations of A_1 and A_2 in Eq. (A6) in Appendix A. The total AR coefficient A in Fig. 7 equals to 1 when $E < \Delta$ (see the black doted lines), which means that the perfect AR happens in the type-II WSM-superconductor junction even in the presence of a large interface barrier [46].

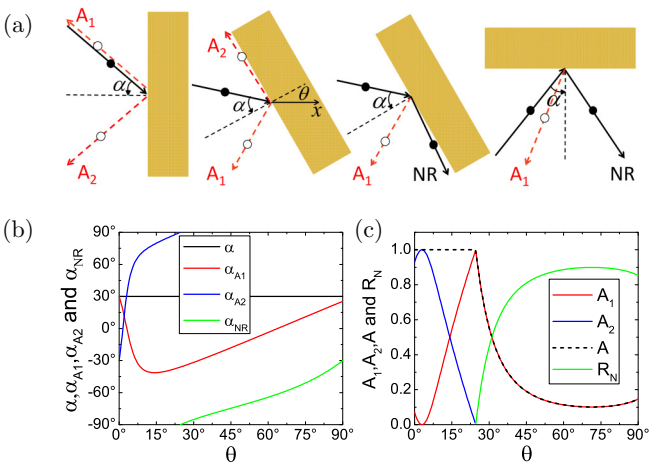

FIG. 8. (a) Schematic diagrams of the AR A_1, A_2, and the normal reflection (NR) when changing the type-II WSM-superconductor interface orientation angle θ. (b) The AR angles α_{A1}, α_{A2}, and normal reflection angle α_{NR} as functions of θ. (c) The coefficients of AR A_1, A_2, A, and normal reflection vs θ. Here the incident angle α is fixed to be 30°, the incident energy $E = 0.5$, $\mu = 0$, and $v_1 = 1.1$.

IV. ANDREEV REFLECTIONS WHEN THE WSM-SUPERCONDUCTOR INTERFACE ORIENTATION ANGLE $\theta \neq 0$

In this section, we consider the case of the nonzero orientation angle ($\theta \neq 0$) of the WSM-superconductor interface. We consider that the normal of the WSM-superconductor interface is still in the x-y plane, but it has an intersection angle θ with the x axis [see Fig. 8(a)]. If the normal of the WSM-superconductor interface is not in the x-y plane, one can do a rotation transformation around the x axis to make the normal in the x-y plane, because the Hamiltonian of the WSM in Eqs. (1) and (2) has rotational symmetry around the x axis. For a finite orientation angle θ, the WSM is in the $x < -y\tan\theta$ region and the superconductor is in the $x > -y\tan\theta$ region. In this case, the incident angle α lies in the range $[\max(-\pi/2, \theta - \alpha_c), \min(\pi/2, \theta + \alpha_c)]$ with $\alpha_c = \arctan(v_2/\sqrt{v_1^2 - v_2^2})$. For example, when $\theta = 0$, the incident angle α lies in the range $[-\alpha_c, \alpha_c]$, while α is restricted within $[\pi/2 - \alpha_c, \pi/2]$ for $\theta = \pi/2$.

In order to calculate the double AR coefficients, we first take a coordinate transformation:

$$\begin{pmatrix} \tilde{x} \\ \tilde{y} \end{pmatrix} = \begin{pmatrix} \cos\theta & \sin\theta \\ -\sin\theta & \cos\theta \end{pmatrix} \begin{pmatrix} x \\ y \end{pmatrix}. \tag{19}$$

After the coordinate transformation, the BdG Hamiltonian in Eq. (3) becomes (for simplicity, we set $p_z = 0$)

$$\tilde{H}_{\mathrm{BdG}} = \begin{pmatrix} H_+(\tilde{p}) - \mu(\tilde{x}) & \Delta(\tilde{x}) \\ \Delta^*(\tilde{x}) & -H_+(\tilde{p}) + \mu(\tilde{x}) \end{pmatrix}, \tag{20}$$

where $H_+(\tilde{p})$ is

$$H_+ = v_1\sigma_0(\tilde{p}_x\cos\theta - \tilde{p}_y\sin\theta) + v_2\sigma_x(\tilde{p}_x\cos\theta - \tilde{p}_y\sin\theta) + v_2\sigma_y(\tilde{p}_x\sin\theta + \tilde{p}_y\cos\theta), \quad (21)$$

where $\tilde{p}_x = -i\hbar\partial_{\tilde{x}}$, $\tilde{p}_y = -i\hbar\partial_{\tilde{y}}$. $\mu(\tilde{x})$ and $\Delta(\tilde{x})$ are, respectively,

$$\mu(\tilde{x}) = \begin{cases} \mu & \tilde{x} < 0 \\ U & \tilde{x} > 0 \end{cases}, \quad \Delta(\tilde{x}) = \begin{cases} 0 & \tilde{x} < 0 \\ \Delta & \tilde{x} > 0 \end{cases}. \quad (22)$$

The energy dispersion in the WSM region is

$$E_{e\pm}(\tilde{k}) = \hbar v_1(\tilde{k}_x\cos\theta - \tilde{k}_y\sin\theta) \pm \hbar v_2|\tilde{k}| - \mu, \quad (23)$$

where $|\tilde{k}| = \sqrt{\tilde{k}_x^2 + \tilde{k}_y^2}$. In the new coordinate system, the WSM and superconductor are respectively in $\tilde{x} < 0$ and $\tilde{x} > 0$ regions, but the band tilts in both $\tilde{x}$ and $\tilde{y}$ directions. Since the energy E and wave vector $\tilde{k}_y$ are conserved upon reflection at the interface $\tilde{x} = 0$, by performing similar calculations as in Sec. III B we can obtain the directions and the amplitudes of the double ARs (see Appendix B).

Figure 8(a) is the schematic diagram of the evolutions of the double ARs A_1 and A_2 when varying the WSM-superconductor interface orientation angle θ at the fixed incident angle $\alpha = 30^\circ$ and incident energy $E = 0.5$. The corresponding reflection angles α_{A1} and α_{A2} are shown in Fig. 8(b). When $\theta = 0$, the retro-AR A_1 has the same angle as the incident angle ($\alpha_{A1} = 30^\circ$), and the specular AR A_2 is symmetric with A_1 with $\alpha_{A2} = -30^\circ$. With the increasing of the orientation angle θ, the retro-AR angle α_{A1} decreases and the specular AR angle α_{A2} increases. At $\theta \approx 2^\circ$, α_{A2} becomes positive, indicating A_2 jumps into the other side of the normal and becomes the retro-AR. Now double retro-ARs occur with both α_{A1} and α_{A2} being positive while $2^\circ \lesssim \theta \lesssim 5^\circ$. At $\theta \approx 5^\circ$, α_{A1} drops from positive to negative, leading to a retro-AR and a specular AR again. Note that now A_2 is retro-AR and A_1 is specular AR. Further increasing θ, α_{A2} goes up straight to 90°, then the AR A_2 disappears at the critical angle $\theta_c = \arccos v_2/v_1$ and the normal electron reflection arises with its reflection angle $\alpha_{\rm NR} = -90^\circ$. At the critical angle θ_c, the double ARs evolve into one specular AR and one normal reflection due to the band tilt in $\tilde{x}$ direction changing from the type-II ($v_1\cos\theta > v_2$) into the type-I ($v_1\cos\theta < v_2$). Note that although the WSM still belongs to the type-II one, only the tilt along the normal direction ($\tilde{x}$ axis) plays a decisive role in generating the double ARs. With further increase of the orientation angle θ from $\theta = \theta_c$, both α_{A1} and $\alpha_{\rm NR}$ go up. Finally, when $\theta = 90^\circ$, the normal reflection angle $\alpha_{\rm NR}$ increases to -30° and A_1 turns back to the retro-AR but with smaller AR angle α_{A1} than α, which is similar with the normal metal-superconductor junction case. Figure 8(c) shows the amplitudes for the double ARs A_1, A_2, and the normal reflection. One can see that both A_1 and A_2 have large value with $A = A_1 + A_2 = 1$ at $\theta < \theta_c$. $A_1 = 1$ and $A_2 = 0$ at the critical angle θ_c. Further increasing θ, A_2 disappears and the normal reflection arises with its coefficient R_N increasing with θ except for θ near 90°. All the analysis above shows the spatial anisotropy of the double ARs.

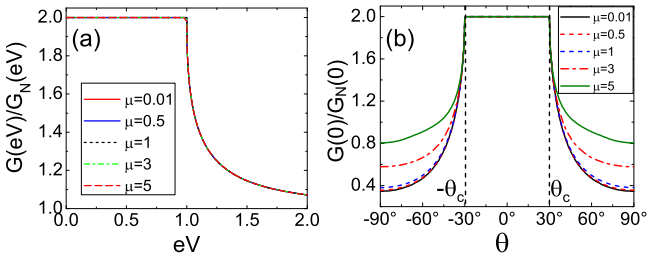

FIG. 9. (a) Conductance $G(eV)$ vs the bias eV with the interface orientation angle $\theta = 0$ and (b) the zero-bias conductance $G(0)$ as a function of θ. The parameter $v_1 = 2/\sqrt{3}$ and the cutoff value $\tilde{q}$ is set to be 30.

V. THE CONDUCTANCE OF THE TYPE-II WSM-SUPERCONDUCTOR JUNCTION

After obtaining the AR and normal reflection coefficients, the differential conductance of the type-II WSM-superconductor junction can be derived from the BTK formula [44]:

$$G(eV) = \frac{2e^2S}{\pi^2h}\int d\tilde{k}_y\int dk_z[1 + A(\tilde{k}_y,k_z,eV) - R_N(\tilde{k}_y,k_z,eV)], \quad (24)$$

with S being the cross-sectional area of the junction. Here the spin and valley degeneracies [47] are already considered. While the interface orientation angle $\theta < \theta_c$, the double ARs still exist and we have the total AR coefficient $A = T^A(E)$, the normal reflection coefficient $R_N = 0$, so the conductance $G(eV)$ can reduce into $\frac{2e^2\tilde{q}^2S}{\pi h}[1 + T^A(eV)]$, where $\tilde{q}$ is the cutoff value of the integral area (i.e., $\tilde{k}_y^2 + k_z^2 \leqslant \tilde{q}^2$). Figure 9(a) shows the conductance $G(eV)$ versus the bias for the angle $\theta = 0$. Here, $G(eV)$ is normalized by the conductance $G_N(eV)$ of the normal junction. One can see that the conductance exhibits a plateau within the superconductor gap and decreases in the same way for different chemical potentials μ, which shows a universal behavior. We also calculate the zero-bias conductance $G(eV = 0)$ as a function of the orientation angle θ [48–50]. A remarkable conductance behavior due to the double ARs can be seen from Fig. 9(b). The zero-bias conductance shows a plateau within the critical angle θ_c, but it decreases quickly when $\theta > \theta_c$ because the normal reflection arises and the total AR coefficient $A < 1$. Increasing μ would moderately enhance the conductance. These unique features are robust against the interface barrier because that the double ARs are not affected by the barrier, which is different from the normal metal-superconductor and graphene-superconductor junctions [34,35,37,44]. Therefore the strong conductance anisotropy that characterizes the type-II WSM-superconductor junction should be unambiguously observable in experiments. What's more, by experimentally observing the critical angle θ_c, the band tilting v_1/v_2, the important parameter of the type-II WSM, can be obtained.

VI. CONCLUSION AND DISCUSSIONS

In conclusion, we investigate the Andreev reflection (AR) at the type-II Weyl semimetal(WSM)-superconductor interface and find a new kind of AR: the double ARs, where for one

incident electron beam, two beams of holes are reflected back. This phenomena is similar to the double reflections of light in anisotropic crystals and shows another opticslike property of the Weyl fermion. A little difference between the double ARs and the optical double reflections is that the reflected holes are in the retro and specular directions of the incident electron respectively, not both in the specular directions. By varying the WSM-superconductor interface orientation angle θ, the directions of the double ARs show strong anisotropy and in some small range of θ we may even observe the double retro-ARs. The essential physical reason behind the double ARs is the violent band tilt in type-II WSMs, so that both interband and intraband electron-hole conversions happen at the interface. Interface barriers has little influence on the double ARs due to the band tilt. The double ARs should be a unique phenomena in type-II WSMs, and we may expect more interesting phenomena associated with the double ARs in type-II WSMs-superconductor hybrid system, such as the Josephson effect, double ARs under magnetic fields, and so on. These findings pave the way to new opticslike phenomenon in quantum transport.

Finally, we also discuss the conductance through the type-II WSM-superconductor junction and find two distinct conductance behaviors, which originate from the double ARs. One is the conductance plateau within the superconductor gap when the interface orientation angle $\theta = 0$ and the other is the zero-bias conductance anisotropy with respect to the orientation angle. Since the system consisting of the WSM coupled with superconductor has been fabricated in experiment, the double ARs and these two remarkable conductance behaviours should be observable in the present technology.

ACKNOWLEDGMENTS

Z.H. thanks P. Lv and Y.-F. Zhou for helpful discussions. This work was financially supported by National Key R and D Program of China (2017YFA0303301), NBRP of China (2015CB921102) and NSF-China under Grants No. 11274364 and No. 11574007.

APPENDIX A: THE DERIVATIONS OF THE DOUBLE AR COEFFICIENTS OF THE WSM-BARRIER-SUPERCONDUCTOR JUNCTION

In this appendix, we give the detailed derivations of the double AR coefficients in the presence of the interface barrier. In the normal WSM region ($x < -d$), the wave function $\Psi(\mathbf{r})$ can be written as

$$\Psi(\mathbf{r}) = \Psi_{e-}(\mathbf{r}) + r_1\Psi_{h+}(\mathbf{r}) + r_2\Psi_{h-}(\mathbf{r}) \tag{A1}$$

with $\Psi_{e-}(\mathbf{r}), \Psi_{h+}(\mathbf{r})$, and $\Psi_{h-}(\mathbf{r})$ defined in Eq. (8). In the barrier region ($-d < x < 0$), the wave function $\Psi(\mathbf{r})$ can be written as

$$\Psi(\mathbf{r}) = c_1\Psi^B_{e+}(\mathbf{r}) + c_2\Psi^B_{e-}(\mathbf{r}) + c_3\Psi^B_{h+}(\mathbf{r}) + c_4\Psi^B_{h-}(\mathbf{r}), \tag{A2}$$

where

$$\begin{aligned}
\Psi^B_{e+}(\mathbf{r}) &= \begin{pmatrix} k^B_+ + k_z \\ k^B_{x+} + ik_y \\ 0 \\ 0 \end{pmatrix} \exp\left(ik^B_{x+}x + ik_y y + ik_z z\right), \\
\Psi^B_{e-}(\mathbf{r}) &= \begin{pmatrix} -k^B_- + k_z \\ k^B_{x-} + ik_y \\ 0 \\ 0 \end{pmatrix} \exp\left(ik^B_{x-}x + ik_y y + ik_z z\right), \\
\Psi^B_{h+}(\mathbf{r}) &= \begin{pmatrix} 0 \\ 0 \\ -k^{B'}_+ + k_z \\ k^{B'}_{x+} + ik_y \end{pmatrix} \exp\left(ik^{B'}_{x+}x + ik_y y + ik_z z\right), \\
\Psi^B_{h-}(\mathbf{r}) &= \begin{pmatrix} 0 \\ 0 \\ k^{B'}_- + k_z \\ k^{B'}_{x-} + ik_y \end{pmatrix} \exp\left(ik^{B'}_{x-}x + ik_y y + ik_z z\right),
\end{aligned} \tag{A3}$$

and

$$\begin{aligned}
k^B_{x\pm} &= \frac{v_1(E - V_0) \mp v_2\sqrt{(E - V_0)^2 + \hbar^2\left(v_1^2 - v_2^2\right)q^2}}{\hbar\left(v_1^2 - v_2^2\right)}, \\
k^{B'}_{x\pm} &= \frac{-v_1(E + V_0) \pm v_2\sqrt{(E + V_0)^2 + \hbar^2\left(v_1^2 - v_2^2\right)q^2}}{\hbar\left(v_1^2 - v_2^2\right)}, \\
k^B_\pm &= \sqrt{{k^B_{x\pm}}^2 + q^2}, \\
k^{B'}_\pm &= \sqrt{{k^{B'}_{x\pm}}^2 + q^2},
\end{aligned} \tag{A4}$$

where $q^2 = k_y^2 + k_z^2$.

In the superconducting region ($0 < x$), the outgoing wave functions $\Psi(\mathbf{r})$ can be written as Eq.(13) in the main text. The wave function $\Psi(\mathbf{r})$ must satisfy the matching conditions at the interfaces $x = -d$ and $x = 0$:

$$\begin{aligned}
\Psi(\mathbf{r})|_{x=-d^-} &= \Psi(\mathbf{r})|_{x=-d^+}; \\
\Psi(\mathbf{r})|_{x=0^-} &= \Psi(\mathbf{r})|_{x=0^+}.
\end{aligned} \tag{A5}$$

Using the above boundary conditions, the AR amplitudes r_1 and r_2, then the AR coefficients A_1 and A_2, can numerically be calculated. After some straightforward but cumbersome algebra, we give the expressions for r_1 and r_2 in the thin barrier limit ($d \to 0$ and $V_0 \to \infty$, but dV_0 remains finite):

$$r_{1/2} = \frac{(k_{x-} + ik_y)(k'_\mp \pm k_z) \pm (k_- - k_z)(k'_{x\mp} + ik_y)}{(k'_+ - k_z)(k'_{x-} + ik_y) + (k'_{x+} + ik_y)(k'_- + k_z)} e^{-i\beta}.$$

The AR coefficients A_1 and A_2 are given as

$$A_{1/2}(E) = \left|\frac{(k'_\pm \mp k_z)(v_1k'_\pm \mp v_2k'_{x\pm})}{(k_- - k_z)(v_1k_- - v_2k_{x-})}\right| |r_{1/2}|^2. \tag{A6}$$

Comparing with the nonbarrier case, one can find that the expressions in Eq. (A6) are exactly the same as Eq. (16) in the main text.

APPENDIX B: THE DERIVATIONS OF THE AR COEFFICIENTS WHEN THE WSM-SUPERCONDUCTOR INTERFACE ORIENTATION ANGLE $\theta \neq 0$

In Appendix B, we give the AR coefficients A_1 and A_2 and their directions when the WSM-superconductor interface orientation angle $\theta \neq 0$. Note that there are two cases need to be considered. The first one is $v_1 \cos\theta > v_2$, where the slopes in the $+\tilde{x}$ direction of the tilted bands for the incident electrons (reflected holes) are all positive (negative), and there exists double ARs at the interface. The second case is $v_1 \cos\theta < v_2$, where the band tilt in the $+\tilde{x}$ direction is not so violent that only one reflected mode exists for holes. In this case, an AR and a normal reflection happen at the WSM-superconductor interface, which is similar to the normal metal-superconductor junction or graphene-superconductor junction.

Next considering an electron incidence from the WSM side to the WSM-superconductor interface with the incident angle α and the incident energy E, and choosing the valence band (E_{e-}) incidence, the modes for incident and reflected electrons (holes) in the WSM region ($\tilde{x} < 0$) can be given as follows:

$$\tilde{\Psi}_{e-} = \begin{pmatrix} -\sqrt{\tilde{k}_{x-}^2 + \tilde{k}_y^2} \\ (\cos\theta + i\sin\theta)\tilde{k}_{x-} - (\sin\theta - i\cos\theta)\tilde{k}_y \\ 0 \\ 0 \end{pmatrix} \times \exp(i\tilde{k}_{x-}\tilde{x} + i\tilde{k}_y\tilde{y}),$$

$$\tilde{\Psi}_{h+} = \begin{pmatrix} 0 \\ 0 \\ -\sqrt{\tilde{k}_{xh+}^2 + \tilde{k}_y^2} \\ (\cos\theta + i\sin\theta)\tilde{k}_{xh+} - (\sin\theta - i\cos\theta)\tilde{k}_y \end{pmatrix} \times \exp(i\tilde{k}_{xh+}\tilde{x} + i\tilde{k}_y\tilde{y}),$$

$$\tilde{\Psi}_{h-} = \begin{pmatrix} 0 \\ 0 \\ \sqrt{\tilde{k}_{xh-}^2 + \tilde{k}_y^2} \\ (\cos\theta + i\sin\theta)\tilde{k}_{xh-} - (\sin\theta - i\cos\theta)\tilde{k}_y \end{pmatrix} \times \exp(i\tilde{k}_{xh-}\tilde{x} + i\tilde{k}_y\tilde{y}), \text{ if } v_1\cos\theta > v_2,$$

$$\tilde{\Psi}_r = \begin{pmatrix} -\sqrt{\tilde{k}_{xr}^2 + \tilde{k}_y^2} \\ (\cos\theta + i\sin\theta)\tilde{k}_{xr} - (\sin\theta - i\cos\theta)\tilde{k}_y \\ 0 \\ 0 \end{pmatrix} \times \exp(i\tilde{k}_{xr}\tilde{x} + i\tilde{k}_y\tilde{y}), \quad \text{if} \quad v_1\cos\theta < v_2, \tag{B1}$$

where the wave vectors for the incident electron and the reflected holes (electron) are

$$\begin{aligned} \tilde{k}_y &= \frac{(E+\mu)(v_1\sin\theta - v_0\sin\alpha)}{\hbar\left[v_1 v_0\cos(\theta-\alpha) - \left(v_1^2 - v_2^2\right)\right]}, \\ \tilde{k}_{x-} &= \frac{(E+\tilde{\mu})\tilde{v}_1 + v_2\sqrt{(E+\tilde{\mu})^2 + \hbar^2\tilde{k}_y^2\left(\tilde{v}_1^2 - v_2^2\right)}}{\hbar\left(\tilde{v}_1^2 - v_2^2\right)}, \\ \tilde{k}_{xr} &= \frac{(E+\tilde{\mu})\tilde{v}_1 - v_2\sqrt{(E+\tilde{\mu})^2 + \hbar^2\tilde{k}_y^2\left(\tilde{v}_1^2 - v_2^2\right)}}{\hbar\left(\tilde{v}_1^2 - v_2^2\right)}, \\ \tilde{k}_{xh\pm} &= \frac{-(E-\tilde{\mu})\tilde{v}_1 \pm v_2\sqrt{(E-\tilde{\mu})^2 + \hbar^2\tilde{k}_y^2\left(\tilde{v}_1^2 - v_2^2\right)}}{\hbar\left(\tilde{v}_1^2 - v_2^2\right)}, \end{aligned} \tag{B2}$$

and we have defined

$$\begin{aligned} v_0 &= v_1\cos(\alpha-\theta) - \sqrt{v_1^2\cos^2(\alpha-\theta) - \left(v_1^2 - v_2^2\right)}, \\ \tilde{v}_1 &= v_1\cos\theta, \quad \tilde{\mu} = \mu + \hbar v_1\sin\theta\tilde{k}_y. \end{aligned} \tag{B3}$$

In Eq. (B1), $\tilde{\Psi}_{e-}$ is the incident mode for electron. The reflected mode $\tilde{\Psi}_{h+}$ for hole always exists regardless of the angle θ, but the other reflected mode $\tilde{\Psi}_{h-}$ for hole keeps only when $v_1\cos\theta > v_2$. If $v_1\cos\theta < v_2$, the normal reflection mode $\tilde{\Psi}_r$ arises, replacing the reflected hole $\tilde{\Psi}_{h-}$. Therefore the wave functions $\Psi(\mathbf{r})$ in the WSM region (the $\tilde{x} < 0$ region) can be written as follows:

$$\Psi(\mathbf{r}) = \begin{cases} \tilde{\Psi}_{e-} + r_1\tilde{\Psi}_{h+} + r_2\tilde{\Psi}_{h-} & \text{if} \quad \tilde{v}_1 > v_2, \\ \tilde{\Psi}_{e-} + r_1\tilde{\Psi}_{h+} + r_{\mathrm{NR}}\tilde{\Psi}_r & \text{if} \quad \tilde{v}_1 < v_2. \end{cases} \tag{B4}$$

Here, r_1, r_2, and r_{NR} are the amplitudes of the AR A_1, the AR A_2 and the normal reflection, respectively.

The outgoing modes in the superconductor region (the $\tilde{x} > 0$ region) are

$$\tilde{\Psi}_{S+} = \begin{pmatrix} e^{i\beta} \\ (\cos\theta + i\sin\theta)e^{i\beta} \\ 1 \\ \cos\theta + i\sin\theta \end{pmatrix} \exp(i\tilde{k}_{x1}\tilde{x} + i\tilde{k}_y\tilde{y} - \tilde{\tau}_1\tilde{x}) \tag{B5}$$

and

$$\tilde{\Psi}_{S-} = \begin{cases} \begin{pmatrix} e^{i\beta} \\ -(\cos\theta + i\sin\theta)e^{i\beta} \\ 1 \\ -(\cos\theta + i\sin\theta) \end{pmatrix} \exp(i\tilde{k}_{x2}\tilde{x} + i\tilde{k}_y\tilde{y} - \tilde{\tau}_2\tilde{x}), \text{ if } \tilde{v}_1 > v_2, \\ \begin{pmatrix} e^{-i\beta} \\ -(\cos\theta + i\sin\theta)e^{-i\beta} \\ 1 \\ -(\cos\theta + i\sin\theta) \end{pmatrix} \exp(i\tilde{k}_{x2}\tilde{x} + i\tilde{k}_y\tilde{y} - \tilde{\tau}_2\tilde{x}), \text{ if } \tilde{v}_1 < v_2. \end{cases} \tag{B6}$$

where

$$\beta = \begin{cases} \arccos(E/\Delta) & \text{if} \quad E < \Delta, \\ -i\,\mathrm{arcosh}(E/\Delta) & \text{if} \quad E > \Delta, \end{cases}$$
$$\tilde{k}_{x1} \simeq \frac{U}{\hbar(v_1\cos\theta + v_2)}, \quad \tilde{k}_{x2} \simeq \frac{U}{\hbar(v_1\cos\theta - v_2)}, \tag{B7}$$
$$\tilde{\tau}_1 = \frac{\Delta\sin\beta}{\hbar(v_1\cos\theta + v_2)}, \quad \tilde{\tau}_2 = \frac{\Delta\sin\beta}{\hbar|v_1\cos\theta - v_2|}.$$

After obtaining the outgoing modes, the wave-function $\Psi(\mathbf{r})$ in the superconductor region (the $\tilde{x} > 0$ region) is

$$\Psi(\mathbf{r}) = a\tilde{\Psi}_{S+} + b\tilde{\Psi}_{S-}, \tag{B8}$$

where a and b are constants to be determined by matching the boundary conditions.

The matching condition at the interface $\tilde{x} = 0$ of the WSM-superconductor junction is $\Psi(\mathbf{r})|_{\tilde{x}=0^-} = \Psi(\mathbf{r})|_{\tilde{x}=0^+}$. For the $v_1\cos\theta > v_2$ case, we have

$$(\tilde{\Psi}_{e-} + r_1\tilde{\Psi}_{h+} + r_2\tilde{\Psi}_{h-})|_{\tilde{x}=0^-} = (a\tilde{\Psi}_{S+} + b\tilde{\Psi}_{S-})|_{\tilde{x}=0^+},$$

and the AR coefficients are

$$A_1 = \left|\frac{\langle\tilde{\Psi}_{h+}|\tilde{J}_x|\tilde{\Psi}_{h+}\rangle}{\langle\tilde{\Psi}_{e-}|\tilde{J}_x|\tilde{\Psi}_{e-}\rangle}\right||r_1|^2, \quad A_2 = \left|\frac{\langle\tilde{\Psi}_{h-}|\tilde{J}_x|\tilde{\Psi}_{h-}\rangle}{\langle\tilde{\Psi}_{e-}|\tilde{J}_x|\tilde{\Psi}_{e-}\rangle}\right||r_2|^2. \tag{B9}$$

On the other hand, for the $v_1\cos\theta < v_2$ case, we have

$$(\tilde{\Psi}_{e-} + r_1\tilde{\Psi}_{h+} + r_{\mathrm{NR}}\tilde{\Psi}_r)|_{\tilde{x}=0^-} = (a\tilde{\Psi}_{S+} + b\tilde{\Psi}_{S-})|_{\tilde{x}=0^+},$$

and the AR coefficient A_1 and normal reflection coefficient R_N are

$$A_1 = \left|\frac{\langle\tilde{\Psi}_{h+}|\tilde{J}_x|\tilde{\Psi}_{h+}\rangle}{\langle\tilde{\Psi}_{e-}|\tilde{J}_x|\tilde{\Psi}_{e-}\rangle}\right||r_1|^2, \quad R_N = \left|\frac{\langle\tilde{\Psi}_r|\tilde{J}_x|\tilde{\Psi}_r\rangle}{\langle\tilde{\Psi}_{e-}|\tilde{J}_x|\tilde{\Psi}_{e-}\rangle}\right||r_{\mathrm{NR}}|^2, \tag{B10}$$

where the particle current density operator is defined as $\tilde{J}_x \equiv \tau_z \otimes [v_1\cos\theta\sigma_0 + v_2\cos\theta\sigma_x + v_2\sin\theta\sigma_y]$. The coefficients in Eqs. (B9) and (B10) can be numerically obtained.

The incident and reflected angles for the electrons and holes are

$$\alpha = -\arctan\left(\frac{\partial E}{\partial\tilde{k}_y}/\frac{\partial E}{\partial\tilde{k}_x}\right), \tag{B11}$$

where E is the energy dispersion for electrons or holes.

[1] C. W. J. Beenakker, Rev. Mod. Phys. **80**, 1337 (2008).
[2] X. Wan, A. M. Turner, A. Vishwanath, and S. Y. Savrasov, Phys. Rev. B **83**, 205101 (2011).
[3] Z. Wang, H. Weng, Q. Wu, X. Dai, and Z. Fang, Phys. Rev. B **88**, 125427 (2013).
[4] L. P. He, X. C. Hong, J. K. Dong, J. Pan, Z. Zhang, J. Zhang, and S. Y. Li, Phys. Rev. Lett. **113**, 246402 (2014).
[5] M. M. Vazifeh and M. Franz, Phys. Rev. Lett. **111**, 027201 (2013); A. A. Burkov, *ibid.* **113**, 247203 (2014); S. A. Parameswaran, T. Grover, D. A. Abanin, D. A. Pesin, and A. Vishwanath, Phys. Rev. X **4**, 031035 (2014); A. C. Potter, I. Kimchi, and A. Vishwanath, Nat. Commun. **5**, 5161 (2014); X. Huang, L. Zhao, Y. Long, P. Wang, D. Chen, Z. Yang, H. Liang, M. Xue, H. Weng, Z. Fang, X. Dai, and G. Chen, Phys. Rev. X **5**, 031023 (2015); Y. Xu, F. Zhang, and C. Zhang, Phys. Rev. Lett. **115**, 265304 (2015).
[6] Q.-D. Jiang, H. Jiang, H. Liu, Q.-F. Sun, and X. C. Xie, Phys. Rev. Lett. **115**, 156602 (2015).
[7] C.-Z. Chen, J. Song, H. Jiang, Q.-F. Sun, Z. Wang, and X. C. Xie, Phys. Rev. Lett. **115**, 246603 (2015).
[8] W. Chen, L. Jiang, R. Shen, L. Sheng, B. G. Wang, and D. Y. Xing, Europhys. Lett. **103**, 27006 (2013).
[9] Q.-D. Jiang, H. Jiang, H. Liu, Q.-F. Sun, and X. C. Xie, Phys. Rev. B **93**, 195165 (2016).
[10] A. Kitaev, Ann. Phys. (NY) **303**, 2 (2003).
[11] L. Fu and C. L. Kane, Phys. Rev. Lett. **100**, 096407 (2008).
[12] B. Q. Lv, Z.-L. Feng, Q.-N. Xu, X. Gao, J.-Z. Ma, L.-Y. Kong, P. Richard, Y.-B. Huang, V. N. Strocov, C. Fang, H.-M. Weng, Y.-G. Shi, T. Qian, and H. Ding, Nature (London) **546**, 627 (2017).
[13] A. A. Soluyanov, D. Gresch, Z. Wang, Q. Wu, M. Troyer, X. Dai, and B. A. Bernevig, Nature **527**, 495 (2015).
[14] M. Alidoust, K. Halterman, and A. A. Zyuzin, Phys. Rev. B **95**, 155124 (2017).
[15] T. E. O'Brien, M. Diez, and C. W. J. Beenakker, Phys. Rev. Lett. **116**, 236401 (2016).
[16] M. Koshino, Phys. Rev. B **94**, 035202 (2016).
[17] Z.-M. Yu, Y. Yao, and S. A. Yang, Phys. Rev. Lett. **117**, 077202 (2016).
[18] S. Tchoumakov, M. Civelli, and M. O. Goerbig, Phys. Rev. Lett. **117**, 086402 (2016).
[19] M. Udagawa and E. J. Bergholtz, Phys. Rev. Lett. **117**, 086401 (2016).
[20] A. A. Zyuzin and R. P. Tiwari, JETP Lett. **103**, 717 (2016).
[21] S.-Y. Xu, N. Alidoust, G. Chang, H. Lu, B. Singh, I. Belopolski, D. S. Sanchez, X. Zhang, G. Bian, H. Zheng, M.-A. Husanu, Y. Bian, S.-M. Huang, C.-H. Hsu, T.-R. Chang, H.-T. Jeng, A. Bansil, T. Neupert, V. N. Strocov, H. Lin, S. Jia, and M. Z. Hasan, Sci. Adv. **3**, e1603266 (2017).
[22] K. Deng, G. Wan, P. Deng, K. Zhang, S. Ding, E. Wang, M. Yan, H. Huang, H. Zhang, Z. Xu, J. Denlinger, A. Fedorov, H. Yang, W. Duan, H. Yao, Y. Wu, S. Fan, H. Zhang, X. Chen, and S. Zhou, Nat. Phys. **12**, 1105 (2016).
[23] A. Tamai, Q. S. Wu, I. Cucchi, F. Y. Bruno, S. Riccò, T. K. Kim, M. Hoesch, C. Barreteau, E. Giannini, C. Besnard, A. A. Soluyanov, and F. Baumberger, Phys. Rev. X **6**, 031021 (2016).
[24] L. Huang, T. M. McCormick, M. Ochi, Z. Zhao, M.-T. Suzuki, R. Arita, Y. Wu, D. Mou, H. Cao, J. Yan, N. Trivedi, and A. Kaminski, Nat. Mater. **15**, 1155 (2016).
[25] F. Y. Bruno, A. Tamai, Q. S. Wu, I. Cucchi, C. Barreteau, A. delaTorre, S. McKeownWalker, S. Ricco, Z. Wang, T. K. Kim, M. Hoesch, M. Shi, N. C. Plumb, E. Giannini, A. A. Soluyanov, and F. Baumberger, Phys. Rev. B **94**, 121112(R) (2016).
[26] C.-L. Wang, Y. Zhang, J.-W. Huang, G.-D. Liu, A.-J. Liang, Y.-X. Zhang, B. Shen, J. Liu, C. Hu, Y. Ding, D.-F. Liu, Y. Hu, S.-L. He, L. Zhao, L. Yu, J. Hu, J. Wei, Z.-Q. Mao, Y.-G. Shi, X.-W. Jia, F.-F. Zhang, S.-J. Zhang, F. Yang, Z.-M. Wang,

Q.-J. Peng, Z.-Y. Xu, C.-T. Chen, and X.-J. Zhou, Chin. Phys. Lett. **34**, 097305 (2017).
[27] C. Wang, Y. Zhang, J. Huang, S. Nie, G. Liu, A. Liang, Y. Zhang, B. Shen, J. Liu, C. Hu, Y. Ding, D. Liu, Y. Hu, S. He, L. Zhao, L. Yu, J. Hu, J. Wei, Z. Mao, Y. Shi, X. Jia, F. Zhang, S. Zhang, F. Yang, Z. Wang, Q. Peng, H. Weng, X. Dai, Z. Fang, Z. Xu, C. Chen, and X. J. Zhou, Phys. Rev. B **94**, 241119(R) (2016).
[28] Y. Wu, D. Mou, N. H. Jo, K. Sun, L. Huang, S. L. Bud'ko, P. C. Canfield, and A. Kaminski, Phys. Rev. B **94**, 121113(R) (2016).
[29] H. Zheng, G. Bian, G. Chang, H. Lu, S.-Y. Xu, G. Wang, T.-R. Chang, S. Zhang, I. Belopolski, N. Alidoust, D. S. Sanchez, F. Song, H.-T. Jeng, N. Yao, A. Bansil, S. Jia, H. Lin, and M. Z. Hasan, Phys. Rev. Lett. **117**, 266804 (2016).
[30] T. Meng and L. Balents, Phys. Rev. B **86**, 054504 (2012).
[31] G. Y. Cho, J. H. Bardarson, Y.-M. Lu, and J. E. Moore, Phys. Rev. B **86**, 214514 (2012).
[32] L. Aggarwal, S. Gayen, S. Das, R. Kumar, V. Süß, C. Felser, C. Shekhar, and G. Sheet, Nat. Commun. **8**, 13974 (2017).
[33] A. F. Andreev, Zh. Eksp. Teor. Fiz. **46**, 1823 (1964) [Sov. Phys. JETP **19**, 1228 (1964)].
[34] Q.-F. Sun, J. Wang, and T.-H. Lin, Phys. Rev. B **59**, 3831 (1999).
[35] Q.-F. Sun and X. C. Xie, J. Phys.: Condens. Matter **21**, 344204 (2009).
[36] U. Khanna, D. K. Mukherjee, A. Kundu, and S. Rao, Phys. Rev. B **93**, 121409(R) (2016).
[37] C. W. J. Beenakker, Phys. Rev. Lett. **97**, 067007 (2006).
[38] S.-G. Cheng, Y. Xing, J. Wang, and Q.-F. Sun, Phys. Rev. Lett. **103**, 167003 (2009); S.-G. Cheng, H. Zhang, and Q.-F. Sun, Phys. Rev. B **83**, 235403 (2011).
[39] Y. Xing, J. Wang, and Q.-F. Sun, Phys. Rev. B **83**, 205418 (2011).
[40] Time-reversal symmetry requires $H_-(\mathbf{k}) = H(-K_0 + k) = \mathcal{T}H(\mathbf{K}_0 - k)\mathcal{T}^{-1} = \mathcal{T}H_+(-\mathbf{k})\mathcal{T}^{-1} = H_+^*(-\mathbf{k})$, where H is the Hamiltonian for the whole Brillouin zone and $\mathcal{T}$ is the time-reversal operator.
[41] P. G. De Gennes, *Superconductivity of Metals and Alloys* (Benjamin, New York, 1966).
[42] H. Ren, L. Liu, D. Liu, and Z. Song, J. Mod. Opt. **52**, 529 (2005).
[43] J. Wu and C. Zhang, Sci. China Ser. G-Phys. Mech. Astron. **52**, 1003 (2009).
[44] G. E. Blonder, M. Tinkham, and T. M. Klapwijk, Phys. Rev. B **25**, 4515 (1982).
[45] S. Bhattacharjee and K. Sengupta, Phys. Rev. Lett. **97**, 217001 (2006).
[46] Q.-F. Sun, Y.-X. Li, W. Long, and J. Wang, Phys. Rev. B **83**, 115315 (2011).
[47] Here for simplicity we assume the Hamiltonian of another Weyl node with negative chirality at K' is $H' = v_1\sigma_0 p_x - v_2\boldsymbol{\sigma}\cdot p$, of which the ARs coefficients A_1 and A_2 are found to be exactly the same as those at K_0.
[48] I. Iguchi, W. Wang, M. Yamazaki, Y. Tanaka, and S. Kashiwaya, Phys. Rev. B **62**, R6131 (2000).
[49] J. Y. T. Wei, N.-C. Yeh, D. F. Garrigus, and M. Strasik, Phys. Rev. Lett. **81**, 2542 (1998).
[50] R. S. Gonnelli, D. Daghero, D. Delaude, M. Tortello, G. A. Ummarino, V. A. Stepanov, J. S. Kim, R. K. Kremer, A. Sanna, G. Profeta, and S. Massidda, Phys. Rev. Lett. **100**, 207004 (2008).